IGARSS 2020 - 2020 IEEE International Geoscience and Remote Sensing Symposium | 978-1-7281-6374-1/20/$31.00 ©2020 IEEE | DOI: 10.1109/IGARSS39084.2020.9324537

TOWARDS A MASS-CONSISTENT METHODOLOGY FOR REALISTIC MELTING HYDROMETEOR RETRIEVAL

Kwo-Sen Kuo[1,2], Adrian M Loftus[1,2], William S Olson[1,3], Robert S Schrom[1,4], Benjamin T Johnson[5], and Ian S Adams[1]

[1]NASA Goddard Space Flight Center, Greenbelt, Maryland, USA
[2]ESSIC, University of Maryland, College Park, Maryland, USA
[3]Joint Center for Earth Systems Technology, University of Maryland, Baltimore County, Maryland, USA
[4]Universities Space Research Association, Columbia, Maryland, USA
[5]University Corporation for Atmospheric Research, Joint Center for Satellite Data Assimilation, College Park, Maryland, USA

ABSTRACT

To address the acute challenge posed by the melting layer to accurate surface precipitation retrievals from space, we ensure the compositional consistency in ice, liquid, and total masses of synthetic melting hydrometeors with a method of stochastic compensation. The method is applied to simulated melting hydrometeors prior to calculating their scattering properties using the discrete dipole approximation (DDA). We investigate the impact of this stochastic compensation to calculated scattering properties by contrasting it with a naïve approach and report our findings.

Index Terms— precipitation remote sensing, melting layer, electromagnetic scattering, spaceborne radar

1. INTRODUCTION

NASA's Global Precipitation Measurement (GPM) mission follows in the successful footsteps of the Tropical Rainfall Measuring Mission (TRMM) and ushers in the era of global spaceborne precipitation remote sensing with an active instrument component, i.e. Precipitation Radar (PR, Ku-band) for TRMM and Dual-frequency Precipitation Radar (DPR, Ku-Ka-band) for GPM. The more global coverage of GPM increases the probability of observing solid- and mixed-phase precipitation, which presents appreciable challenges to space-based precipitation retrievals.

For solid-phase precipitation, Kuo et al [1] and Olson et al [2] have demonstrated a promising strategy for improving the quality of the active (radar) and passive (radiometer) combined retrievals of snowfall. They have achieved consistency in radar-radiometer combined retrievals by incorporating electromagnetic (EM) scattering properties obtained from complex, realistic synthetic snow particles. We thus intend to build on the success and adopt the same general strategy to improve the combined retrieval of mixed-phase precipitation, i.e. starting with realistic synthetic melting hydrometeors and followed by calculation of scattering properties obtained from efficient EM scattering methods.

We first describe in section 2, the algorithm used to simulate hydrometeor melting for this study. We discuss in section 3 the compositional inconsistency issues caused by the discrete nature of the melting algorithm and associated post processing. Section 4 describes similar compositional inconsistencies associated with the attempt to optimize EM scattering computation efficiency. Next, we introduce in section 5 our innovative stochastic compensation method for addressing the compositional inconsistency issues. We examine and report in section 6 the impact of stochastic compensation by contrasting it with a naïve alternative. Finally, we conclude with planned future efforts in section 7.

2. SINGLE PARTICLE MELTING MODEL (SPMM)

The Single Particle Melting Model (SPMM) performs physics-based particle melting simulations on an integer-indexed three-dimensional (3D) Cartesian grid. Each occupied cell in the grid represents a small, but finite unit of volume of either ice or liquid. This assemblage of ice and liquid water grid cells constitutes the particle volume.

The basis for melting and melt-water movement in SPMM occurs through nearest-neighbor interactions. In a 3D domain, any given grid cell has 26 nearest neighbors (including all diagonals). The interaction distance is limited to one neighbor, simplifying the computational requirements of the algorithm. Fig. 1 illustrates the melting process in two dimensions; the same logic applies to the 3D model. The melting simulation proceeds iteratively, in the following

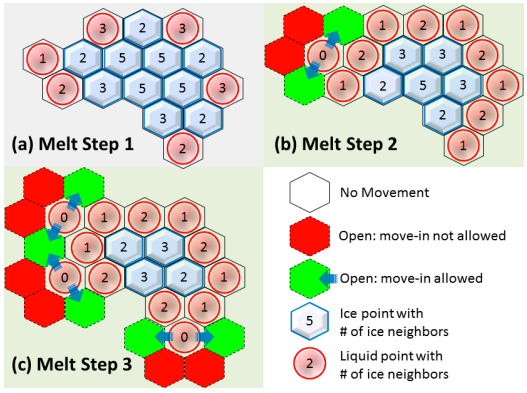

Fig. 1 A simplified diagram depicting the steps in the SPMM. At each step, ice elements (blue) are converted to liquid (red) following nearest neighbor rules (see text). Numbers denote the number of nearest ice neighbors. Panel (a) indicates the first iteration of the melting algorithm, (b) shows the second iteration, and the allowable move conditions, and (c) shows the third iteration, where more ice has melted and three cells are now free to move into the green regions.

steps, until all ice is melted and a nearly spherical droplet is formed.

1. Populate a 3-D Cartesian grid with "ice" grid cells using synthetic aggregates of [1].
2. Iterate over all ice grid cells, tabulating all 26 nearest neighbors (6, 12, and 8 opposite to facets, edges, and vertices respectively, excluding self).
3. The ice grid cell having the fewest ice neighbors are melted (see Fig. 1a). A stochastic factor is employed to control the rate of melting.
4. After each melt iteration, a movement check is applied to those liquid points having zero ice neighbors. Prohibiting the movement of liquid elements that do have ice neighbors simulates a "coating" effect; whereas liquid elements with no ice neighbors are allowed to move (Fig. 1**b** and **c**).
5. Movement is a weighted random walk, subject to certain constraints. The walk is weighted toward total particle center of mass, simulating the coalescence of liquid water. The movement phase iterates until all moving liquid cannot move to an open space closer to the center of mass than the current position. Return to step 2.

In this simple model, collapse, breakup, or water shedding of the particle are not simulated – any orphaned droplets created during melting are migrated towards the center of total mass as cohesive droplets. Fig. 2 visualizes an example melting simulation using SPMM for a snow aggregate with an equivalent mass diameter (D_m) of 2.6 mm.

SPMM provides melting simulations for any arbitrary particle shape until it is completely melted. The melting increments and distribution of melt-water can be finely-tuned to suit the application. On a modern desktop computer, a particle having 200,000 ice grid cells (or "dipoles" in DDA parlance) can complete the entire melting process in less than 5 minutes using a single processor core.

3. POST-SPMM PROCESSING AND ISSUES

There are a couple of complicating issues that impact hydrometeor geometric and compositional consistency arising from SPMM and post processing. We list them below.

A. The SPMM grid cells represent a constant volume. When an ice cell melts into water, it is assumed to occupy the same cell volume. Thus, in the SPMM melting process, the mass of the hydrometeor gradually and slightly increases because liquid water has a higher density (~9%), violating mass conservation.

B. To ensure orientational consistency for scattering calculation and later reference, the synthetic melting hydrometeor is reoriented according to its moments of inertia, aligning the axis corresponding to the maximum inertia with the vertical direction, i.e. the direction of incoming pulse from the spaceborne radar. Digitally, such a reorientation is carried out with the integer-indexed 3D Cartesian grid of SPMM using floating-point numbers for rotation angles. The rotated grid is then cast back into another integer-indexed 3D Cartesian grid, thereby introducing discretization errors and minute variation to mass and composition (i.e. solid ice versus liquid water).

Issues A and B introduce relatively small inconsistencies to mass and composition compared to that from issue C described in the next section.

4. ISSUE WITH DIPOLE SIZE

Since DDA allows for more versatility with the geometry and composition of scattering targets (melting hydrometeors in this case) than most of the other methods, it is an obvious choice for calculating the scattering properties of complicated melting aggregates. The (linear) dipole size, d (related also to the grid cell size used to specify the synthetic hydrometeor in SPMM), is a crucial factor in configuring DDA calculations. For the DDA solution to converge with accurate angular cross sections, it is recommended that $d < \lambda/(4\pi|m|)$, where λ is the wavelength and m the index of refraction of the target. However, the computational cost of popular DDA codes, such as ADDA [3] and DDSCAT [4], is proportional to $N \ln N$, where N is the number of dipoles. For the same target volume, N is proportional to d^{-3}. That is, doubling the dipole size will lead to a factor of 8 reduction in N and, in turn, a factor of ~16 reduction in computational cost. Thus, to optimize the usage of computational resource when conducting DDA calculations for large hydrometeors across a number of frequencies, we should adapt d according to wavelength/frequency (and index of refraction), instead of using a fixed dipole size throughout, because using the same dipole size recommended for a higher frequency at a lower frequency may simply incur a large computation cost without benefit.

C. To maximize computational efficiency, it is logical to "blur" (i.e. coarsen) the original cell/dipole size used for

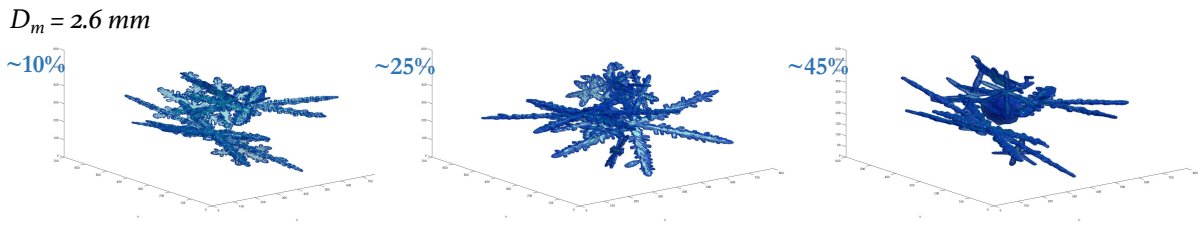

Fig. 2 Snapshots of SPMM simulated melting of a hydrometeor with liquid-equivalent D_m = 2.6 mm, at ~0.1 (10%), ~0.25 (25%), and ~0.45 (45%) liquid mass fractions. (Note: A different perspective is used to render the hydrometeor at ~25% liquid mass fraction.)

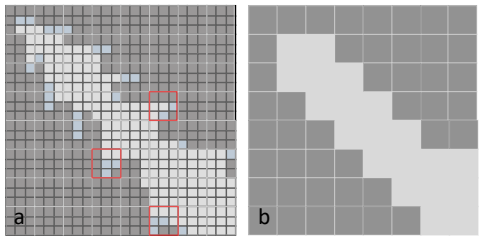

Fig. 3 The consequences of volume-majority blurring illustrated with a two-dimensional example. (a) A dendritic arm in original, fine resolution with melted tips (in pale blue). (b) The same dendritic arm after 3^2 (3×3) blurring, where melted water has been eliminated.

the grid to represent the synthetic hydrometeors (suitable for higher frequencies) to a larger dipole size appropriate for lower frequencies. However, naïve blurring not only changes the morphology of the hydrometeor but also causes violation of mass and composition conservation.

Fig. 3 illustrates the consequence of a naïve volume-majority rule, i.e. the composition of a blurred cell is the water phase that occupies the highest volume. We see that the blurring not only changes the shape of the dendritic arm but also eliminates its melted tips, violating mass and composition conservation.

5. STOCHASTIC COMPENSATION

To address the mass and composition issues, i.e. A and B for SPMM post-processing and C for dipole size adjustment, we developed *stochastic compensation*.

In the SPMM post-processing, we address the cumulative effect of issues A and B together. We compute and record the mass of the all-ice snowflake aggregate before the melting simulation starts by multiplying the ice-occupied volume with ice density. At the completion of the melting simulation, we go through each stage in the melting sequence and compare the mass of melting hydrometeor at that stage to the initial mass. Ice or liquid mass is then stochastically adjusted, i.e. added to or removed from it depending on the difference, to maintain mass and composition (i.e. solid ice and liquid water mass fractions) consistency. Adjustment sites are determined by the number of occupied facet neighbors (1-6 for a cube). Mass removal occurs irrespective of neighbor type, with cells on the particle surface (i.e., those having fewer neighbors) removed first. On the other hand, liquid/ice mass addition aims to fill in gaps within liquid/ice regions (i.e., cells having 5, 4 liquid/ice neighbors). Note that mass removal dominates stochastic compensation.

We also apply a similar stochastic compensation to blurring, i.e. coarsening resolution (C). That is, the composition of the blurred volume is set stochastically with a probability equal to the constituent volume fractions. For example, with a 3^3 blurring, every block of $3^3 = 27$ original cells are aggregated into one blurred cell. If, out of the 27 cells, there are g, i, and l cells ($g + i + l = 27$) of air, ice, and liquid water respectively, the blurred cell constituent volume fractions are thus $g/27$, $i/27$, and $l/27$ for air, ice, and liquid water. What actually fills the blurred cell is determined by a random number, which is designed to give probabilities of air, ice, and liquid water equal to the constituent volume fractions. As a consequence of the law of large numbers in probability, we expect stochastic compensation to be more effective when there are more heterogeneous blurred cells for it to apply.

The stochastic compensation approach yields much better (total) mass conservation as demonstrated in Fig. 4, where curves of fractional mass change compared to the starting snow particle mass for naïve volume-majority (solid line) and stochastic (dashed line) approaches with 2^3 (red), 3^3 (blue), and 6^3 (green) blurring are plotted for a simulated melting sequence (i.e. the one depicted in Fig. 2) as the liquid fraction increases (horizontal axis).

6. RESULTS

Fig. 5 shows the impact of stochastic compensation applied to SPMM post-processing on liquid mass fraction (LMF, the ratio of liquid to total mass) and on orientation-averaged (over 544 orientations) Ku-band (13.5 GHz) cross sections, i.e. C_e

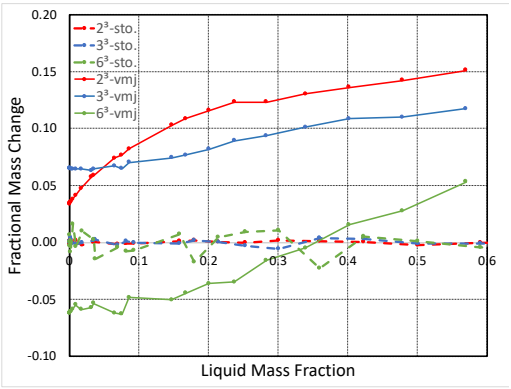

Fig. 4 Comparing volume-majority (solid) and stochastic compensation (dashed) in preserving total mass relative to the starting mass of the hydrometeor depicted in Fig. 2 for 2^3 (red), 3^3 (blue), and 6^3 (green) blurring.

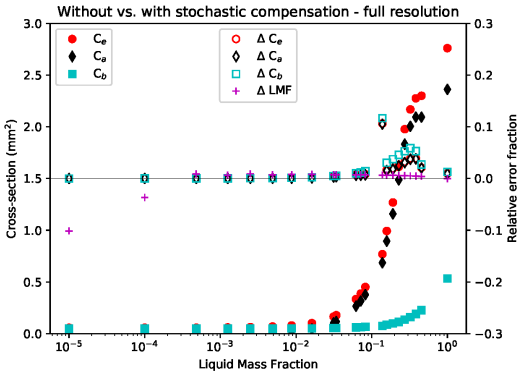

Fig. 5 Effects of stochastic compensation on liquid mass fraction (LMF) and Ku-band extinction, absorption, and backscatter cross sections, C_e, C_a, and C_b, respectively, for the hydrometeor depicted in Fig. 2. (See text for details.)

(extinction), C_a (absorption), and C_b (backscatter). The horizontal axis denotes the progression of simulated melting with liquid water fraction in logarithmic scale. The cross-section values of the stochastically compensated particles are plotted using filled symbols (i.e. circles, diamonds, and squares for C_e, C_a, and C_b, respectively) against the vertical axis on the left, whereas the relative differences to the stochastically compensated, i.e. ΔC_e, ΔC_a, and ΔC_b are plotted using corresponding hollow symbols and plus signs (+) for ΔLMF, against the axis on the right. The relative difference in LMF is generally very small, except for the early stages of melting at the beginning of the sequence, when the number of melted cells is small and stochastic compensation is less effective. For LMF < 0.1, the difference in cross sections remains negligible despite large ΔLMF, whereas the largest discrepancies occur around 0.2 < LMF < 0.5 where ΔLMF is small.

The effect of 6^3 blurring on C_e, C_a, C_b, and LMF is shown in Fig. 6, which follows the same convention used in Fig. 5. While stochastic compensation maintains satisfactory mass and composition conservation, except at the early melting stages, the relative differences in cross sections between full and blurred resolutions are deleteriously large, reaching nearly 80% (0.8) around LMF of 0.2-0.3.

We initially hypothesized that the large discrepancies were primarily caused by the severe 6^3 blurring factor, which may

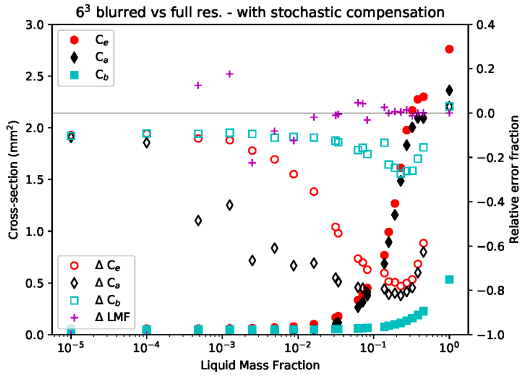

Fig. 6 Similar to **Error! Reference source not found.**, but for e ffects of 6^3 blurring on Ku-band cross sections and LMF.

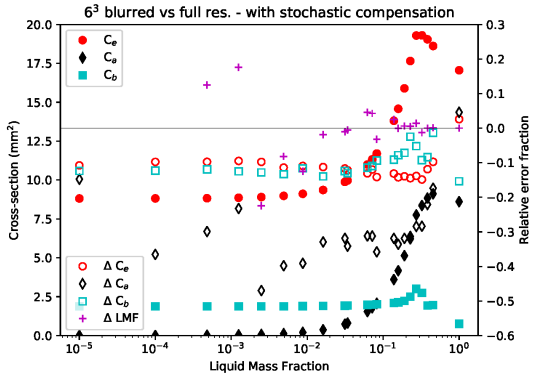

Fig. 7 Similar to Fig. 6 but for W-band.

Table 1 Refractive indices of liquid water and ice at -10°C for Ku-, Ka-, and W-bands.

	Ku	Ka	W
Water	$6.26 + i\,2.98$	$4.07 + i\,2.37$	$2.94 + i\,1.39$
Ice	$1.79 + i\,3.61\ 10^{-4}$	$1.79 + i\,9.13\ 10^{-4}$	$1.79 + i\,2.41\ 10^{-3}$

have extensively altered the spatial distribution of liquid water and ice. However, at W-band (see Fig. 7), the discrepancies are considerably smaller. We also discover that the magnitudes of relative errors at Ka-band (not shown) are between those of Ku- and W-bands. Examination of the refractive indices at these bands (Table 1**)** indicates that refractive index contrast between ice and water is perhaps an even better predictor of the relative errors than altered spatial distribution of liquid water and ice.

7. CONCLUSIONS AND FUTURE PLANS

Stochastic compensation provides a viable means to preserve mass and composition conservation for simulated hydrometeor melting and dipole resolution adjustment. We present here a first look at its impact contrasted with a naïve approach with which mass and composition conservation can be badly violated. However, stochastic compensation does not appear to preserve accuracy in scattering properties, especially with blurring. We plan to investigate further as to which factors contribute more towards the uncertainty in scattering properties, refractive index contrast or altered spatial distribution of liquid water and ice, by using different blurring factors and examining composition spatial distributions.

REFERENCES

[1] K.-S. Kuo, W. S. Olson, B. T. Johnson, M. Grecu, L. Tian, T. L. Clune, B. H. van Aartsen, A. J. Heymsfield, L. Liao, and R. Meneghini, "The Microwave Radiative Properties of Falling Snow Derived from Nonspherical Ice Particle Models. Part I: An Extensive Database of Simulated Pristine Crystals and Aggregate Particles, and Their Scattering Properties," J Appl Meteorol Clim, vol. 55, no. 3, pp. 691–708, Feb. 2016.

[2] W. S. Olson, L. Tian, M. Grecu, K.-S. Kuo, B. T. Johnson, A. J. Heymsfield, A. Bansemer, G. M. Heymsfield, J. R. Wang, and R. Meneghini, "The Microwave Radiative Properties of Falling Snow Derived from Nonspherical Ice Particle Models. Part II: Initial Testing Using Radar, Radiometer and In Situ Observations," J. Appl. Meteorol. Clim., vol. 55, no. 3, pp. 709–722, Jan. 2016.

[3] M. A. Yurkin and A. G. Hoekstra, "The discrete-dipole-approximation code ADDA: Capabilities and known limitations," J Quant Spectrosc Radia Transfer, vol. 112, no. 13, pp. 2234–2247, Sep. 2011.

[4] P. J. Flatau and B. T. Draine, "Fast near field calculations in the discrete dipole approximation for regular rectilinear grids," Opt. Express, OE, vol. 20, no. 2, pp. 1247–1252, 2012.